Multifeature Texture Analysis for the Classification of Clouds in Satellite Imagery

Christodoulos I. Christodoulou, Silas C. Michaelides, and Constantinos S. Pattichis, *Senior Member, IEEE*

***Abstract*—The aim of this work was to develop a system based on multifeature texture analysis and modular neural networks that will facilitate the automated interpretation of satellite cloud images. Such a system will provide a standardized and efficient way for classifying cloud types that can be used as an operational tool in weather analysis. A series of 98 infrared satellite images from the geostationary satellite METEOSAT7 were employed, and 366 cloud segments were labeled into six cloud types after combined agreed observations from ground and satellite. From the segmented cloud images, nine different texture feature sets (a total of 55 features) were extracted, using the following algorithms: statistical features, spatial gray-level dependence matrices, gray-level difference statistics, neighborhood gray tone difference matrix, statistical feature matrix, Laws' texture energy measures, fractals, and Fourier power spectrum. The neural network self-organizing feature map (SOFM) classifier and the statistical K-nearest neighbor (KNN) classifier were used for the classification of the cloud images. Furthermore, the classification results of the nine different feature sets were combined, improving the classification yield for the six classes, for the SOFM classifier to 61% and for the KNN classifier to 64%.**

***Index Terms*—Classification, clouds, K-nearest neighbor (KNN), satellite images, self-organizing feature map (SOFM), texture.**

I. Introduction

GEOSTATIONARY satellites have long been established as excellent cloud-observing platforms for various meteorological applications, primary of which is short-range weather forecasting. Cloud patterns observed from such satellites are interpreted from expert meteorologists and are used in conjunction with several other weather forecasting tools in their day-to-day practice [1]. Clouds are customarily classified in three decks (etages): as low, medium, or high, depending, among several other criteria, on the observed shape of the cloud and the distance of the cloud base from the ground. This kind of classification has been internationally agreed and used by meteorological services worldwide. The cloud identification, by using the combined ground and satellite observations, is further complicated by the fact that the weather-observers report the cloud as seen from below (i.e., from the earth's surface), whereas the satellite senses remotely the cloud from above (i.e., from space). In order to avoid the confusion, which may arise because of this discrepancy in the "observation" point of view, only areas on the satellite image with a single deck of cloud were analyzed in the present research.

Because the interpretation of satellite images by individual weather forecasters implies a high level of personal estimation and subjectivity, artificial neural networks [2] and texture analysis have been employed in previous work, in order to establish an objective methodology for such an interpretation [1], [3]–[6]. Welch *et al.* [3] used texture features like the spatial gray-level dependence matrices (SGLDMs) by Haralick [7] and gray-level difference statistics (GLDS) by Wenska [8] on images from the LANDSAT orbiting satellite. Lee *et al.* [4] used neural networks and the K-nearest neighbor (KNN) classifiers for the classification of clouds in three classes with an overall cloud identification accuracy of 93%, whereas Bankert [5], [6] used a probabilistic neural network (PNN) for the classification of Advanced Very High Resolution Radiometer (AVHRR) imagery. Neural networks use in image texture analysis and in cloud classification has also been shown in [9] where the PNN and the self-organizing feature map (SOFM) classifiers were examined with the singular value decomposition (SVD), and wavelet packet (WP) transformations, and the SGLDM and spectral features. They reported an overall classification accuracy of 91% for the SVD features, after a postprocessing scheme that utilized the contextual information in the satellite images, where similar results were found for the WP and SGLDM features.

The original aspects of this work are the following.

1) The cloud images were obtained by the geostationary satellite METEOSAT7 at 36 000 km, whereas most of the images used in previous work were recorded from orbiting satellites with orbits about 180 km above the earth [3]–[6]. The use of geostationary satellites is considered to be more consistent than that of orbiting satellites. On the one hand, geostationary satellites observe the same geographical area and from the same height, at all times. On the other hand, images from geostationary satellites are more frequent (every half hour) compared to the much less frequent images from orbiting satellites. Therefore, the development of an operational automated technique for the identification of cloud could more easily be adapted to imagery from geostationary satellites, especially in conjunction with appropriate image animation software.
2) The labeling of the different cloud cases was carried out by combined agreed observations from ground and satellite.
3) A large number (55) of texture features was investigated using the following algorithms: statistical features, spatial gray-level dependence matrices, gray-level difference

Manuscript received May 5, 2002; revised April 29, 2003.

C. I. Christodoulou and C. S. Pattichis are with the Department of Computer Science, University of Cyprus, 1678 Nicosia, Cyprus (e-mail: cschr2@ucy.ac.cy; pattichi@ucy.ac.cy).

S. C. Michaelides is with the Meteorological Service, 1418 Nicosia, Cyprus (e-mail: silas@ucy.ac.cy).

Digital Object Identifier 10.1109/TGRS.2003.815404

statistics, neighborhood gray tone difference matrix, statistical feature matrix, Laws' texture energy measures, fractals, and the Fourier power spectrum.

4) A modular architecture incorporating a combiner with weighted averaging was developed, which improved significantly the overall correct classifications score. Moreover, the use of a correction factor is proposed for handling classification problems with unequal class distributions.

II. Data

The satellite images used in the present study originate from the thermal infrared channel onboard the Geostationary satellite METEOSAT7. This thermal infrared channel operates within the range of 10.5–12.5 μm. It detects infrared radiation from the underlying earth's surface and atmosphere within this range, and it has a great advantage over visible radiation channels, as it can be used equally well, day or night. Cold high clouds with low infrared radiance appear white, whereas warmer low-level clouds appear gray, while land and sea, with high infrared radiance, will look relatively dark. The resolution of the infrared radiometer at the subsatellite point amounts to 5 km^2. However, due to the curvature of the earth this resolution decreases toward the outer edges of the image. The satellite images consist of the 0000, 0600, 1200, and 1800 UTC images, corresponding to the main synoptic observing times and which are performed on the basis of internationally agreed standards. The satellite images were contrasted to the actual observations reported at the earth's surface at the above times. These observations are plotted on the respective synoptic maps and archived by the Meteorological Office of Cyprus. Using this standardized information from the human observers on the ground and the expertise of a meteorologist, cloud types were identified on the satellite images and classified manually accordingly.

From a total number of 98 satellite images, 366 samples were manually classified by the expert meteorologist into the following six cloud types:

- altocumulus-altostratus (ACAS);
- cumulonimbus (CB);
- cirrus-cirrostratus (CICS);
- cumulus-stratocumulus (CUSC);
- stratus (ST);
- clear conditions (CLEAR)

For the cloud type ACAS, 52 samples were collected, for CB 13, for CICS 73, for CUSC 126, for ST 34 and for CLEAR 68. Some of these cloud types like CUSC, ACAS and CICS are group types representing cloud usually observed together. It should be emphasized that the labeling of the different cases was carried out after combined agreed observations from ground and satellite. The cloud region of interest was manually outlined and saved for feature extraction. The outline and identification of the cloud was carried out very carefully by the expert meteorologist, in order to include only one type of cloud and in order to avoid including in the segmented image any land borderlines. Fig. 1 shows an infrared satellite image from the geostationary satellite METEOSAT7 and Fig. 2 illustrates examples of segmented cloud images for the six classes.

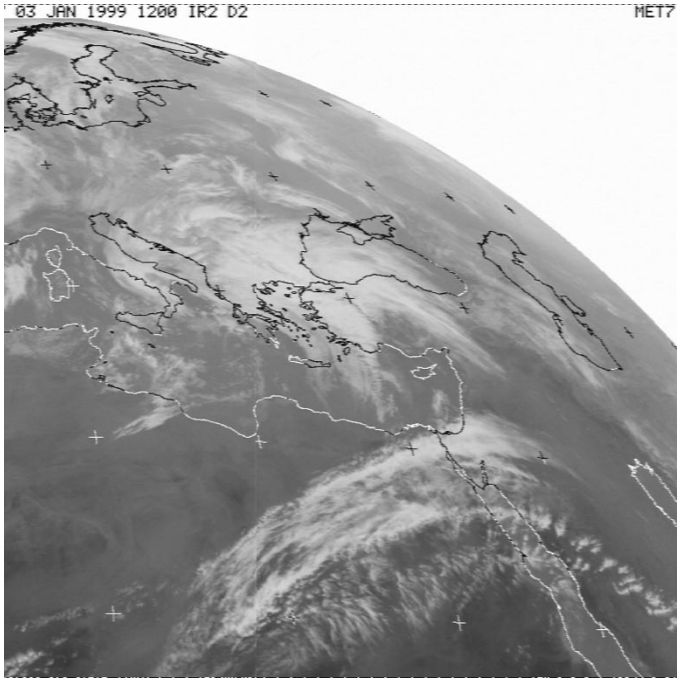

Fig. 1. Infrared satellite image from the geostationary satellite METEOSAT7 (© 2003 EUMETSAT).

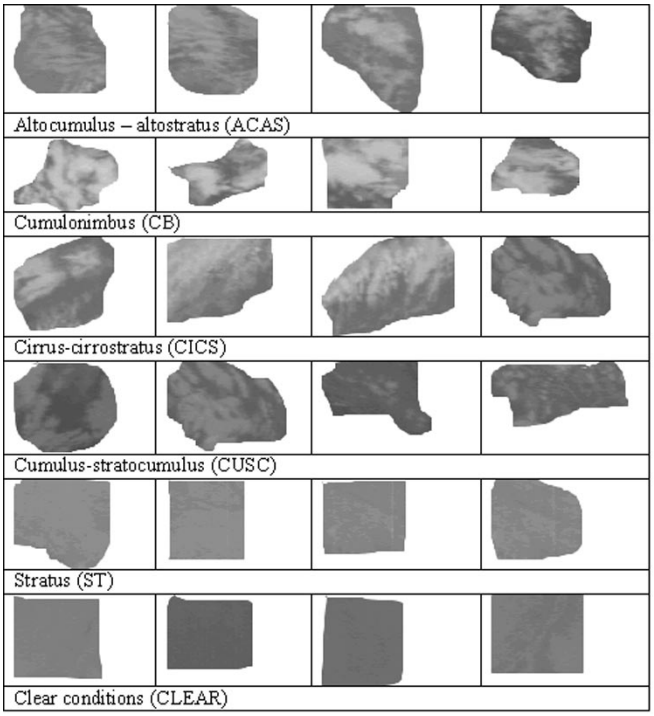

Fig. 2. Examples of segmented cloud images.

III. Texture Feature Extraction

In the feature extraction module multiple texture features were extracted from the manually classified samples, in order to be used for the classification. Texture contains important information, which is used by humans for the interpretation and the analysis of many types of images. Texture refers to the spatial interrelationships and arrangement of the basic elements

of an image [10]. Visually, these spatial interrelationships and arrangements of the image pixels are seen as variations in the intensity patterns or gray tones. Therefore, texture features have to be derived from the gray tones of the image. Although it is easy for humans to recognize texture, it is quite a difficult task to be defined, and subsequently to be interpreted by digital computers.

From the segmented satellite images used in this study, nine different texture feature sets (a total of 55 features) were extracted. The used texture features briefly outlined below were also used successfully in previous work for the classification of ultrasound images of carotid plaques [11].

A. Statistical Features (SF)

The following statistical features were computed [12]:

1) mean value;
2) median value;
3) standard deviation;
4) skewness;
5) kurtosis.

B. Spatial Gray-Level Dependence Matrices (SGLDM)

The SGLDMs as proposed by Haralick *et al.* [7] are based on the estimation of the second-order joint conditional probability density functions that two pixels (k, l) and (m, n) with distance d in direction specified by the angle θ have intensities of gray-level i and gray-level j. Based on the probability density functions, the following texture measures [7] were computed:

1) angular second moment;
2) contrast;
3) correlation;
4) sum of squares: variance
5) inverse difference moment;
6) sum average;
7) sum variance;
8) sum entropy;
9) entropy;
10) difference variance;
11) difference entropy;
12) and 13) information measures of correlation.

For a chosen distance d (in this work $d = 1$ was used) and for angles $\theta = 0^o$, 45°, 90°, and 135° we computed four values for each of the above 13 texture measures. In this work, the mean and the range of these four values were computed for each feature, and they were used as two different feature sets.

C. Gray-Level Difference Statistics (GLDS)

The GLDS algorithm [8] uses first order statistics of local property values based on absolute differences between pairs of gray levels or of average gray levels in order to extract the following texture measures:

1) contrast;
2) angular second moment;
3) entropy;
4) mean.

The above features were calculated for pixel displacements $\delta = (0,1),(1,1),(1,0),(1,-1)$, where $\delta \equiv (\Delta x, \Delta y)$, and their mean values were taken.

D. Neighborhood Gray Tone Difference Matrix (NGTDM)

Amadasun and King [10] proposed the neighborhood gray tone difference matrix in order to extract textural features, which correspond to visual properties of texture. The following features were extracted, for a neighborhood size of 3×3:

1) coarseness;
2) contrast;
3) business;
4) complexity;
5) strength.

E. Statistical Feature Matrix (SFM)

The statistical feature matrix [13] measures the statistical properties of pixel pairs at several distances within an image, which are used for statistical analysis. Based on the SFM the following texture features were computed:

1) coarseness;
2) contrast;
3) periodicity;
4) roughness.

The constants L_r, L_c which determine the maximum intersample spacing distance were set in this work to $L_r = L_c = 4$.

F. Laws Texture Energy Measures (TEM)

For the Laws texture energy measures extraction [14], [15], vectors of length $l = 7$, $L = (1,6,15,20,15,6,1)$, $E = (-1,-4,-5,0,5,4,1)$, and $S = (-1,-2,1,4,1,-2,-1)$ were used, where L performs local averaging, E acts as edge detector, and S acts as spot detector. If we multiply the column vectors of length l by row vectors of the same length, we obtain Laws' $l \times l$ masks. In order to extract texture features from an image, these masks are convolved with the image and the statistics (e.g., energy) of the resulting image are used to describe texture. The following texture features were extracted:

1) LL—texture energy from LL kernel;
2) EE—texture energy from EE kernel;
3) SS—texture energy from SS kernel;
4) LE—average texture energy from LE and EL kernels;
5) ES—average texture energy from ES and SE kernels;
6) LS—average texture energy from LS and SL kernels.

G. Fractal Dimension Texture Analysis (FDTA)

Mandelbrot [16] developed the fractional Brownian motion model in order to describe the roughness of natural surfaces. The Hurst coefficient $H^{(k)}$ [15] was computed for image resolutions $k = 1, 2, 3$. A smooth surface is described by a large value of the parameter H whereas the reverse applies for a rough surface.

H. Fourier Power Spectrum (FPS)

The radial sum and the angular sum of the discrete Fourier transform [8] were computed in order to describe texture.

The algorithms were developed and executed in MATLAB R12 by MathWorks. Table I tabulates the number of features per set and indicative processing time needed to compute the features for an image of 53×59 pixels on a 1.5-GHz Pentium 4 personal computer with 512-MB RAM.

For each of the nine feature sets extracted, a classifier was developed, followed by a combining module that combined the outputs of the nine classifiers. This architecture formed the multifeature/multiclassifier modular neural network system [2] that is described in Sections IV and V. Building a classifier based on an optimal feature selection among the 55 texture features extracted was not investigated in this study because this approach was followed by our group in a similar problem for the classification of medical ultrasound images of the carotid plaque based on texture analysis, and it yield poorer classification results [11] compared to the modular neural network system proposed in this study. The feature selection procedures tested were based on the interclass distance, or on more elaborate techniques like forward and backward selection. Through these techniques some features, which were highly dependent with features in other feature sets, were eliminated.

TABLE I
NUMBER OF FEATURES PER SET AND INDICATIVE PROCESSING TIME NEEDED TO COMPUTE THE FEATURES FOR AN IMAGE OF 53×59 PIXELS ON A 1.5-GHz PENTIUM 4 PERSONAL COMPUTER WITH 512-MB RAM

	Feature Set	*No of Features*	*Processing Time [s]*
1	SF	5	0.032
2	SGLDM (mean)	13	0.343
3	SGLDM (range)	13	0.343
4	GLDS	4	0.094
5	NGTDM	5	0.109
6	SFM	4	0.062
7	TEM	6	0.015
8	FDTA	3	0.390
9	FPS	2	0.078
	Total	*55*	*1.466*

IV. CLASSIFICATION

The classification was implemented using the neural network self-organizing feature map (SOFM) classifier [17], and the statistical KNN classifier [18]. The leave-one-out method was used for evaluating the classification yield, where at each time a single pattern from the dataset was evaluated in relation to the remaining 365 patterns. The SOFM was chosen because it is an unsupervised learning algorithm where the input patterns are freely distributed over the output node matrix [17]. The weights are adapted without supervision in such a way, so that the density distribution of the input data is preserved and represented on the output nodes. This mapping of similar input patterns to output nodes, which are close to each other, represents a discretization of the input space, allowing a visualization of the distribution of the input data. Unsupervised learning is an advantage in case of overlapping classes (like ACAS with CICS and ST with CLEAR), compared to supervised learning algorithms like the back propagation (BP) or the radial basis function (RBF), which cannot easily converge and cannot be trained efficiently, thus providing poorer classification results. Fig. 3 illustrates the distribution of each class on a 12×12 SOFM using as input all the 55 features. The figure illustrates the high degree of overlap between some of the six different classes.

The SOFM was unsupervised trained for 5000 epochs with the 366 cloud patterns, i.e., the pattern labels were not revealed to the network during training. After the training, each pattern (whose label is actually known) was assigned to one of the 144 output nodes of a 12×12 matrix, based on the similarity (Euclidean distance) of the pattern vector to the weight vectors of the trained SOFM. Similar patterns were assigned to the same or neighboring output nodes performing a kind of clustering of the input patterns. The classification for each pattern was implemented based on the class labels of the other patterns in a window 3×3 around the winning node where the test pattern was assigned. So, the test pattern was considered to belong to the majority of the rest of the patterns assigned in the 3×3 window neighborhood. Patterns assigned on the neighboring nodes were given less weight, i.e., their number was multiplied with 0.5 for the four nodes perpendicular to the winning node and with 0.3536 for the four nodes diagonally located. Because in this work the number of patterns per class was unequal, a bias was created in favor of the classes with a large number of members. In order to alleviate the above bias, the number of counted patterns on the node for each class, was multiplied with a correction factor. The correction factor was computed as the total number of patterns, (i.e., 366) divided by the number of members of each class. Thus, classes with a smaller number of members were given a greater weight in the classification process.

The above procedure was repeated for each one of the 366 cloud patterns, using as input vector the nine different feature sets, i.e., nine different SOFM classifiers were trained and evaluated. Furthermore, modular neural networks [2], [19] were used in order to improve the overall system's performance. According to Haykin [2], a neural network is said to be modular, if the computation performed by the network can be decomposed into modules or subsystems, which operate on distinct inputs without communicating with each other. In this paper, the modular neural network was implemented by combining the outputs of the nine different SOFM classifiers, trained with the nine different texture feature sets, using the following combining techniques: 1) majority voting and 2) weighted averaging. In the majority voting, the input pattern was assigned to the class of the majority of the nine classification results. In the weighted averaging case, the six class percentages of the number of patterns per class assigned in the 3×3 neighborhood of the winning output node, were summed up for the nine classifiers sets. The input pattern was assigned to the class with the greatest percentage value.

The statistical KNN classifier was also implemented and used for cloud classification. In the KNN algorithm, the k nearest

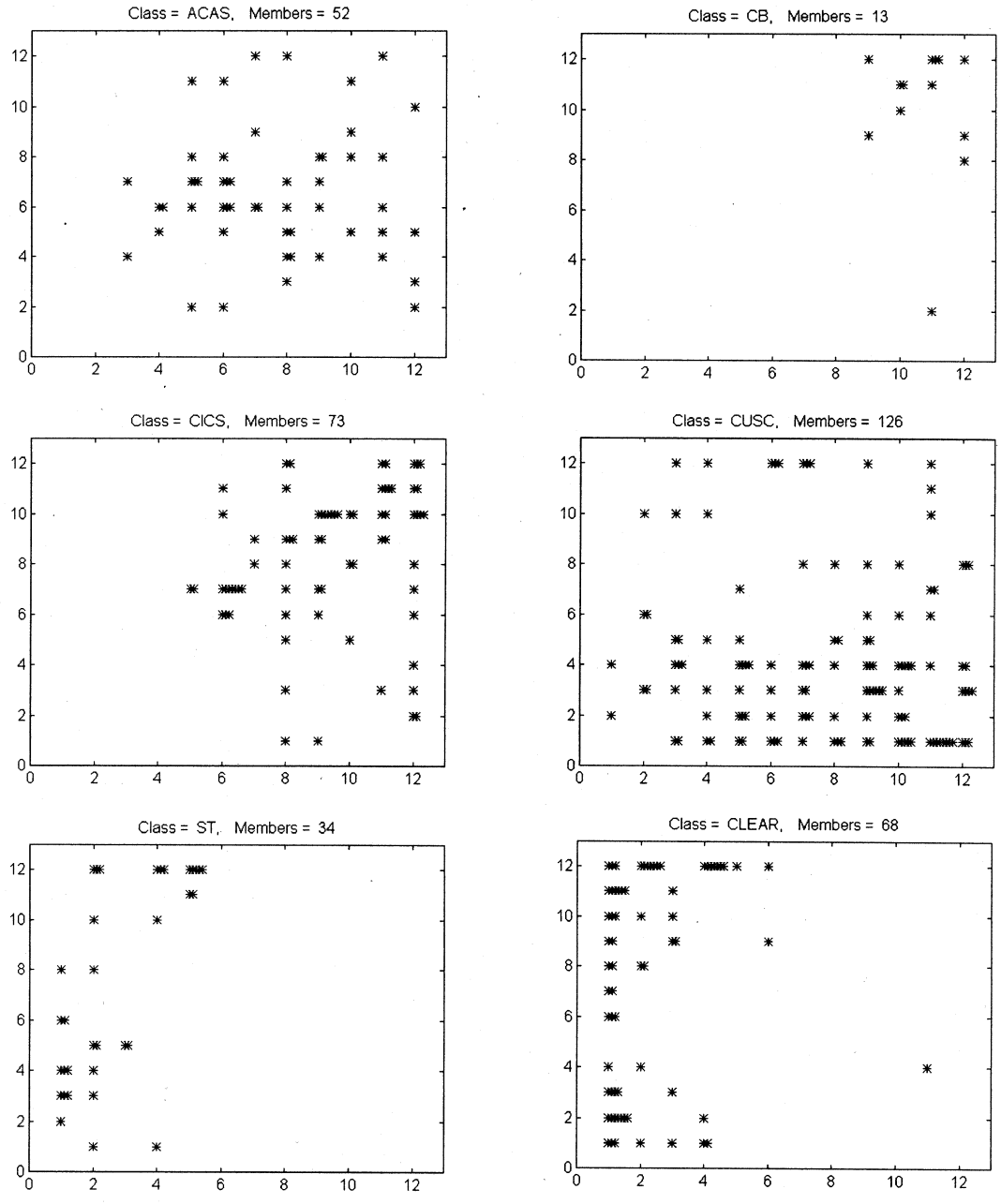

Fig. 3. Distribution of the six cloud classes on a 12 × 12 SOFM matrix using as input all 55 texture features. The figure illustrates the overlap among the different classes.

neighbors of the test pattern were identified, based on their Euclidean distance. The test pattern was assigned to the class of majority of its k neighbors. The classification was implemented in a similar way to the SOFM classifier, using a correction factor and combining techniques. For the KNN classifier, best results were obtained with $k = 3$.

V. Results

Table II tabulates the classification results for the SOFM and the KNN classifiers, for the nine texture feature sets and their average, as well as when the nine classification results were combined with majority voting and with weighted averaging. In the SOFM case, the classification results tabulated represent the average of three different runs in order to obtain a more reliable estimate for the correct classification score. Best results were obtained with the KNN classifier, with an average yield for the nine feature sets of 50.2% of cloud images correctly classified for the six classes, whereas the SOFM classifier yielded 44.7%. The feature sets that gave the highest correct classifications score for the KNN classifier were the SGLDMs (mean) with 60.7%, followed by the SFs with 57.9% and the NGTDMs with 54.1%. For the SOFM, the feature sets with the highest correct classification score were also the SGLDMs (mean) with 57.1%, followed by the NGTDMs with 52.6%, the SFs with 52.2%, and the GLDS with 51.5%. The classification yield for

TABLE II
CLASSIFICATION RESULTS OF THE CLOUD CLASSIFICATION SYSTEM

	Feature Set	*SOFM (%)*	*KNN (%)*
1	SF	52.2	57.9
2	SGLDM (mean)	57.1	60.7
3	SGLDM (range)	48.1	51.1
4	GLDS	51.5	53.0
5	NGTDM	52.6	54.1
6	SFM	42.8	52.2
7	TEM	41.7	51.9
8	FDTA	35.3	44.3
9	FPS	21.4	26.2
	Average	44.7	50.2
	Combine with majority voting	54.5	61.2
	Combine with weighted averaging	60.7	64.2

TABLE III
CONFUSION MATRIX OF THE CLASSIFICATION RESULTS AMONG THE SIX DIFFERENT CLASSES, FOR THE KNN CLASSIFIER AND FOR THE SGLDMs (MEAN) FEATURE SET, WHICH GAVE THE BEST RESULTS

Cloud Class	*Classified as (%)*					
	ACAS	*CB*	*CICS*	*CUSC*	*ST*	*Clear*
ACAS	46.2	9.6	26.9	13.5	0.0	3.8
CB	7.7	46.2	46.2	0.0	0.0	0.0
CICS	26.0	20.5	45.2	8.2	0.0	0.0
CUSC	15.9	2.4	3.2	66.7	5.6	4.0
ST	2.9	0.0	0.0	5.9	82.4	8.8
Clear	4.4	0.0	0.0	5.9	20.6	69.1

both systems was significantly improved when combined with majority voting, and when combined with weighted averaging. For the KNN system, the yield was also improved to 61.2% with majority voting, and 64.2% with weighted averaging, whereas for the SOFM system to 54.5% with majority voting, and 60.7% with weighted averaging. The significant improvement of the classification yield in the combined results can be attributed to the relative large number of six classes. Due to that, misclassifications were distributed to a large number of classes and, hence, when combined easily compensated. Table III tabulates a confusion matrix of the classification results for the KNN classifier, for the SGLDMs (mean) feature set that yielded the best results. As seen from the table, the ACAS clouds were most often misclassified as CICS and vice versa, whereas the same occurred with the ST and the CLEAR classes. These results are in agreement with the pattern distribution displayed in Fig. 3, and with the visual observation of the images as shown in Fig. 2.

VI. CONCLUSION

In this work, multifeature, multiclassifier analysis was used for the classification of satellite cloud images received from an operational geostationary meteorological satellite. The developed system was able to correctly classify cloud images with a success rate of 64% for the six classes. The importance of this work stems from the fact that the satellite cloud images utilized were labeled after a respective ground observation, in an effort to develop a system which will be able to classify clouds based on their satellite images and which classification will be in agreement with the ground observation. Such a system will facilitate the automated objective interpretation of satellite cloud images and can be used as an operational tool in weather analysis. For the classification, combining techniques with the neural SOFM classifier and the statistical KNN classifier were used, whereas the KNN performed better than the SOFM with 64% compared to 61%. The texture feature sets SGLDM, NGTDM, GLDS, and SF, which performed well for cloud classification, also performed well in a similar study for carotid plaques ultrasound images classification [11]. The classification success rate in this work was lower compared to the success rate reported in other studies carried out using neural networks and texture analysis for cloud classification [4], [9]. This can be attributed to the different datasets used and to the labeling of the cloud regions using combined ground and satellite observations. This seems to make the classification more difficult since the weather observers report the cloud as seen from below (i.e., from the earth's surface), whereas the satellite senses remotely the cloud from above (i.e., from space). In conclusion, the results of the present work show that texture features can be successfully used for cloud classification and that a relatively good clustering of the different classes is provided. Furthermore, combining techniques with multiple feature sets and multiple classifiers can further improve the classification yield of the system.

REFERENCES

[1] J. E. Peak and P. M. Tag, "Toward automated interpretation of satellite imagery for navy shipboard applications," *Bull. Amer. Meteorol. Soc.*, vol. 73, no. 7, pp. 995–1008, July 1992.
[2] S. Haykin, *Neural Networks—A Comprehensive Foundation*. New York: Macmillan, 1999.
[3] R. M. Welch, K. S. Kuo, and S. K. Sengupta, "Cloud and surface textural features in polar regions," *IEEE Trans. Geosci. Remote Sensing*, vol. 28, pp. 520–528, July 1990.
[4] J. Lee, R. Weger, S. K. Sengupta, and R. M. Welch, "A neural network approach to cloud classification," *IEEE Trans. Geosci. Remote Sensing*, vol. 28, pp. 846–855, Sept. 1990.
[5] R. L. Bankert, "Cloud classification of AVHRR imagery in maritime regions using a probabilistic neural network," *J. Appl. Meteorol.*, vol. 33, no. 8, pp. 909–918, Aug. 1994.
[6] R. L. Bankert and D. W. Aha, "Improvement to a neural network cloud classifier," *J. Appl. Meteorol.*, vol. 35, no. 11, pp. 2036–2039, Nov. 1996.
[7] R. M. Haralick, K. Shanmugam, and I. Dinstein, "Texture features for image classification," *IEEE Trans. Syst., Man., Cybern.*, vol. SMC-3, pp. 610–621, Nov. 1973.
[8] J. S. Weszka, C. R. Dyer, and A. Rosenfeld, "A comparative study of texture measures for terrain classification," *IEEE Trans. Syst., Man. Cybern.*, vol. SMC-6, Apr. 1976.
[9] B. Tian, M. Shaikh, M. Azimi-Sadjadi, T. V. Haar, and D. Reinke, "A study of cloud classification with neural networks using spectral and textural features," *IEEE Trans. Neural Networks*, vol. 10, pp. 138–151, Jan. 1999.

[10] M. Amadasun and R. King, "Textural features corresponding to textural properties," *IEEE Trans. Syst., Man, Cybern.*, vol. 19, pp. 1264–1274, Sept.–Oct. 1989.
[11] C. I. Christodoulou, C. S. Pattichis, M. Pantziaris, and A. Nicolaides, "Texture-based classification of atherosclerotic cartoid plaques," *IEEE Trans. Med. Imag.*, vol. 22, pp. 902–912, July 2003.
[12] W. H. Press, B. P. Flannery, S. A. Teukolsky, and W. T. Vetterling, *Numerical Recipes, The Art of Scientific Computing*. Cambridge, U.K.: Cambridge Univ. Press, 1987.
[13] C.-M Wu and Y.-C. Chen, "Statistical feature matrix for texture analysis," *Graph. Models Image Process.*, vol. 54, no. 5, pp. 407–419, Sept. 1992.
[14] K. I. Laws, "Rapid texture identification," *SPIE*, vol. 238, pp. 376–380, 1980.
[15] C.-M Wu, Y.-C. Chen, and K.-S. Hsieh, "Texture features for classification of ultrasonic liver images," *IEEE Trans. Med. Imag.*, vol. 11, pp. 141–152, June 1992.
[16] B. B. Mandelbrot, *The Fractal Geometry of Nature*. San Francisco, CA: Freeman, 1982.
[17] T. Kohonen, "The self-organizing map," *Proc. IEEE*, vol. 78, pp. 1464–1480, Sept. 1990.
[18] J. T. Tou and R. C. Gonzalez, *Pattern Recognition Principles*. Reading, MA: Addison-Wesley, 1974.
[19] M. P. Perrone, "Averaging/modular techniques for neural networks," in *The Handbook of Brain Theory and Neural Network*, M. A. Arbib, Ed. Cambridge, MA: MIT Press, 1995, pp. 126–129.

Christodoulos I. Christodoulou received the diploma in electrical engineering with specialization in telecommunications from the Technical University RWTH Aachen, Aachen, Germany, in 1987, and the Ph.D. degree in electronics engineering from the Queen Mary University of London, London, U.K., in 2000.

He carries out his research work in cooperation with the Department of Computer Science, University of Cyprus, Nicosia, Cyprus, and the Cyprus Institute of Neurology and Genetics. His research interests include intelligent information systems, artificial neural networks, signal and image processing, pattern recognition, biosignal analysis, and computer applications in medicine.

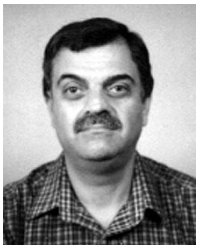

Silas C. Michaelides received the B.Sc. degree in mathematics from the University of Thessaloniki, Thessaloniki, Greece, in 1973, the Masters degree in agricultural meteorology from the University of Reading, Reading, U.K., in 1983, the Masters degree in public sector management from the Cyprus International Institute of Management, Nicosia, Cyprus, in 1992, and the Ph.D. degree in meteorology from the University of Thessaloniki, Thessaloniki, Greece, in 1984.

He is currently with the Meteorological Service of Cyprus, Nicosia, since 1974. His has done research on a wide range of meteorological issues, including applications of artificial neural networks in meteorology.

Constantinos S. Pattichis (S'88–M'88–SM'99) was born on January 30, 1959, in Cyprus. He received the diploma as a technician engineer from the Higher Technical Institute in Cyprus, the B.Sc. in electrical engineering from the University of New Brunswick, Saint John, NB, Canada, the M.Sc. degree in biomedical engineering from the University of Texas, Austin, the M.Sc. degree in neurology from the University of Newcastle Upon Tyne, Newcastle, U.K., and the Ph.D. degree in electronic engineering from the University of London, London, U.K.

He is currently a Senior Scientist and Co-Director of the Department of Computational Intelligence, Cyprus Institute of Neurology and Genetics, Nicosia, Cyprus, as well as an Associate Professor with the Department of Computer Science, University of Cyprus. His current research interests include medical imaging, biosignal analysis, intelligent systems, and health telematics. He has published 30 refereed journal and 80 conference papers in these areas.

Dr. Pattichis has served as Chairperson of the Cyprus Association of Medical Physics and Biomedical Engineering (1996–1998) and the IEEE Cyprus Section (1998–2000). He was Guest Co-Editor of the Special Issue on Emerging Health Telematics Applications in Europe of the IEEE TRANSACTIONS ON INFORMATION TECHNOLOGY IN BIOMEDICINE and was Co-Chairman of MEDICON'98 and MELECON'2000.